between Point Reyes and Point Arena are composed mainly of fine silt derived from the Russian River outflow and have mean grain sizes in the range 30 to 125 μm.
13. D. E. Drake and D. A. Cacchione, *Cont. Shelf Res.* **4–5**, 495 (1985).
14. B. H. Jones, C. N. K. Mooers, M. Reinecker, T. P. Stanton, L. Washburn, *J. Geophys. Res.* **96**, 22207 (1991); R. R. Hood, M. R. Abbot, A. Huyer, *ibid.*, p. 14769.
15. The vertical density gradient is expressed as the buoyancy frequency N and is a measure of the static stability of the water column. It is defined by

$$N = \left(-\frac{g\partial\rho}{\rho\partial z} \right)^{1/2}$$

where g is the acceleration of gravity, ρ is seawater density, and z is the vertical coordinate, positive upward. Vertical density gradients are estimated from moving centered differences of ρ and z over vertical scales of about 4 m followed by smoothing with a running mean over a 12-m vertical scale.
16. S. J. Lentz and J. H. Trowbridge, *J. Phys. Oceanogr.* **21**, 1186 (1991); S. R. Ramp, R. W. Garwood, C. O. Davis, R. L. Snow, *J. Geophys. Res.* **96**, 14947 (1991).
17. D. E. Drake and D. A. Cacchione, *J. Geophys. Res.* **92**, 1699 (1987).
18. D. A. Cacchione and D. E. Drake, *Geo-Mar. Lett.* **6**, 147 (1986).
19. A recent comprehensive review of sediment transport on continental shelves is given by D. A. Cacchione and D. E. Drake, in *The Sea* (Wiley, New York, 1990), vol. 9, chap. 21.
20. The length L scale over which the layer advected is estimated from the distance along the drifter track from the point at which it crossed the continental shelf break to station 218 where the sediment layer was observed, about 80 km. An advective speed U of 0.1 m/s is estimated by assuming that the speed within the layer is similar to the geostrophic current speed in the velocity section of Fig. 3 at the layer depth. The advection time scale L/U is about 9 days.
21. G. S. E. Lagerloef, *J. Geophys. Res.* **97**, 12557 (1992).
22. Suspended sediment concentration is derived from transmissometer and bottle sample data for the Russian River shelf reported in figures 3 and 5 and table 2 of (*17*). An approximately linear relation is found between the beam attenuation coefficient c in reciprocal meters and suspended sediment mass concentration C in milligrams per liter of the form $c = 0.475C + 0.37$ (SE 0.14 m^{-1}).
23. The scale for the width of the region containing resuspended sediments is estimated from the maximum distance the drifter moves inshore of the continental shelf break (200-m isobath) and is about 10 km. Turbidity layers of this scale have been observed on this shelf (*17*).
24. The carbon content of sediments is indicated by their combustible fraction, which is also an indicator of phytoplankton abundance. Suspended sediment samples obtained over the Russian River shelf have combustible fractions in the range of 8 to 53% (*17*). In the CTZ experiment a few bottom turbidity layers exhibited weak but measurable levels of fluorescence, which suggests that they contained phytoplankton that had previously settled to the sea floor.
25. The CTZ Experiment was funded by the Coastal Sciences Program of the Office of Naval Research. The Northern California Coastal Circulation Study was funded by the Minerals Management Service (U.S. Department of the Interior) and was conducted in collaboration with EG&G Washington Analytical Services Center, Inc. D. Lawson of the University of California, Santa Barbara, produced the final satellite images.

7 April 1993; accepted 12 July 1993

Chicxulub Multiring Impact Basin: Size and Other Characteristics Derived from Gravity Analysis

Virgil L. Sharpton, Kevin Burke, Antonio Camargo-Zanoguera, Stuart A. Hall, D. Scott Lee, Luis E. Marín, Gerardo Suárez-Reynoso, Juan Manuel Quezada-Muñeton, Paul D. Spudis, Jaime Urrutia-Fucugauchi

The buried Chicxulub impact structure in Mexico, which is linked to the Cretaceous-Tertiary (K-T) boundary layer, may be significantly larger than previously suspected. Reprocessed gravity data over Northern Yucatán reveal three major rings and parts of a fourth ring, spaced similarly to those observed at multiring impact basins on other planets. The outer ring, probably corresponding to the basin's topographic rim, is almost 300 kilometers in diameter, indicating that Chicxulub may be one of the largest impact structures produced in the inner solar system since the period of early bombardment ended nearly 4 billion years ago.

The Chicxulub structure is widely considered to be an impact crater related to the ~65-Ma (million years ago) K-T boundary layer (*1–3*). Because this feature is buried under 300 to 1100 m of Tertiary carbonate rocks in the Northern Yucatán Platform, geophysical exploration is essential to understand its morphology and structure. Indeed, concentric patterns in gravity and magnetic field data over this feature led to its discovery (*1*). Hildebrand *et al.* (*2*) later recognized two concentric rings in gridded gravity data then available and interpreted their 180-km-diameter outer ring as the rim crest of Chicxulub. They could not resolve concentric structure in the northern one-third of the feature, however, and proposed that an east-northeast trending fault had removed the crater's signature in this region (*2, 4*). To better understand the nature of the Chicxulub impact structure and its regional setting, we compiled and analyzed a new gravity anomaly map (*5*) of northern Yucatán (Figs. 1 and 2).

The gravity data set comprises 3134 offshore measurements and 3675 land stations (Fig. 2A) between 19.5°N to 22.5°N and 88°W to 90.5°W (*6*). After removing obviously spurious points, we gridded the data by a bivariate interpolation scheme designed for irregularly distributed points (*7*). Gravity anomalies in the mapped region range from −16.4 mgal (10^{-5} m s^{-2}) to +53.6 mgal.

The Chicxulub basin is a broad, nearly circular region in which gravity values are 20 to 30 mgal lower than regional values. A distinct 15- to 20-mgal high occupies the geometric center that we place at 21.3°N and 89.6°W (Figs. 1 and 2). Analysis of radial profiles compiled for each 10° increment of azimuth clearly reveals multiple rings expressed as local maxima in the gravity anomaly data. Besides the central gravity high, we recognize three major rings and evidence of a fragmentary fourth ring (Figs. 1, 2, and 3). Basins with three or more concentric rings are the largest impact landforms observed on planetary surfaces. Analyses of multiring impact basins on all the silicate planets of the inner solar system have shown that the radial positions of these topographic rings follow a "square root of 2" spacing rule (*8*). The concentric gravity highs within the Chicxulub basin (Figs. 1 and 2) also follow this spacing rule (Table 1), indicating that they correspond to topographic rings of this now-buried impact basin.

The central gravity high most likely reflects the mass concentration associated with the dense impact melt sheet and the uplift of silicate basement rocks in the middle of the structure. The concentric gravity trough separating the central dome from the inner ring (Fig. 1, ring 1) could mark the position where the dense melt rock sequence is thin enough for the low-density breccias filling the crater to dominate the gravity expression. The diameter of the inner ring is 105 ± 10 km. Ring 1 probably corresponds to the topographic central-peak ring associated with the structural uplift of large complex impact craters (*9*).

Gravity values increase substantially and abruptly between ~70 and ~100 km from the basin center. Near the inside edge of

V. L. Sharpton, D. S. Lee, P. D. Spudis, Lunar and Planetary Institute, 3600 Bay Area Boulevard, Houston, TX 77058.
K. Burke and S. A. Hall, Department of Geosciences, University of Houston, Houston, TX 77004.
A. Camargo-Zanoguera and J. M. Quezada-Muñeton, Gerencia Divisional de Programación y Evaluación, Petróleos Mexicanos, Marina Nacional 329, Mexico City, Mexico 01131.
L. E. Marín, G. Suárez-Reynoso, J. Urrutia-Fucugauchi, Instituto de Geofisica, Universidad Nacional Autónoma de México, Mexico City, Mexico 04510.

this zone of steep gravity gradients, some profiles show local gravity highs or inflections that constitute a partial ring (Fig. 1, ring 2) which is best expressed to the southwest and east (Fig. 2, profile 90). A well-developed third ring, corresponding to the outer ring of (2), is located at the crest of the steep gradients. Although this ring has been interpreted as the rim crest of the Chicxulub crater (2), the steep gravity gradients immediately inside it are not predicted with the shallow deformation characteristic of terrace and rim zones of large impact basins (9). More likely, such gradients mark the outward extent of deep excavation and deformation associated with the transient crater before its collapse during the late stages of the impact process (*10, 11*). Interpretations of the surface morphology of lunar multiring basins also place the deep transient crater boundary between the second and third rings (*11, 12*). These results indicate that a reasonable estimate of the transient crater diameter (D_t) of Chicxulub is ~170 ± 25 km. Impact crater scaling relations derived from computations and experiments (*11*) suggest, therefore, that the Chicxulub-forming impact event excavated to a depth of ~17 to 20 km and that the transient crater was 45 to 60 km deep.

The broad gravity low defining the Chicxulub basin extends out to a distance of ~140 km from the center where the fourth and outermost ring in our data set is located (Table 1). Analyses of the gravity anomalies over other terrestrial impact craters indicate that the edge of the circular low defines the position of the topographic rim (*13*). Ring 4 is expressed as a subtle, discontinuous pattern of local gravity highs that average ~2.5 mgal in amplitude (Fig. 3). The relatively weak expression of this ring in gravity data is consistent with the shallower deformation characteristic of the outer regions of large impact basins (9). Identification is also hampered by data voids within the map area (Fig. 2A) and lack of accessible data west of 90.5°W.

Ring 4 could be somewhat larger than we estimate because the limited data coverage to the west and north does not permit the full extent of the gravity low (the ring's inner flank) to be determined. In calculating the average diameter of this ring, we therefore used the maximum extent of those profiles not reaching the outer edge of the gravity low. Scaling relations derived from observations of large multiring basins on the moon (*11, 12*) and studies of terrestrial complex craters (9), ranging up to 100

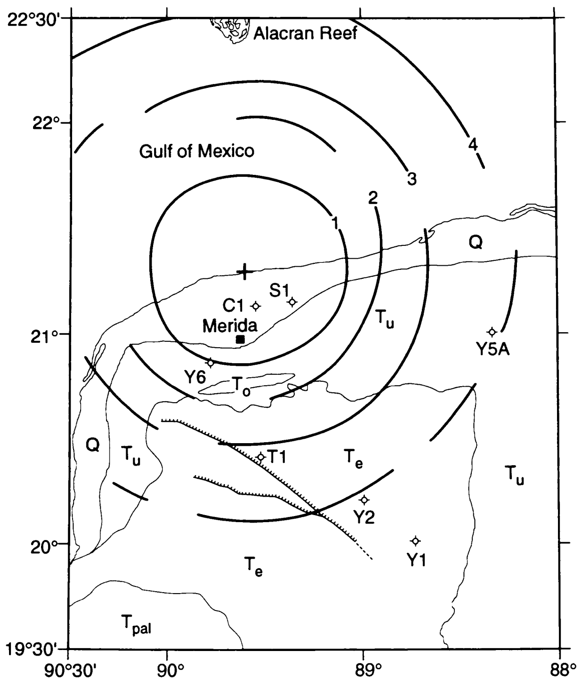

Fig. 1. Surface geology and rings of the Chicxulub multiring basin, Yucatán, Mexico. The three wells that penetrated impact melt rocks and breccias beneath the carbonate cover rocks are C1 (Chicxulub 1), S1 (Sacapuc 1), and Y6 (Yucatán 6). Other well sites shown are Yucatán 1 (Y1), Yucatán 2 (Y2), Yucatán 5A (Y5A), and Ticul 1 (T1). Carbonate units at the surface are Q (Quaternary; <2 Ma), T_u (Upper Tertiary; 2 to 35 Ma), T_e (Eocene; 35 to 55 Ma), and T_{pal} (Paleocene; 55 to 65.0 Ma). Hatchured lines represent the Ticul fault system.

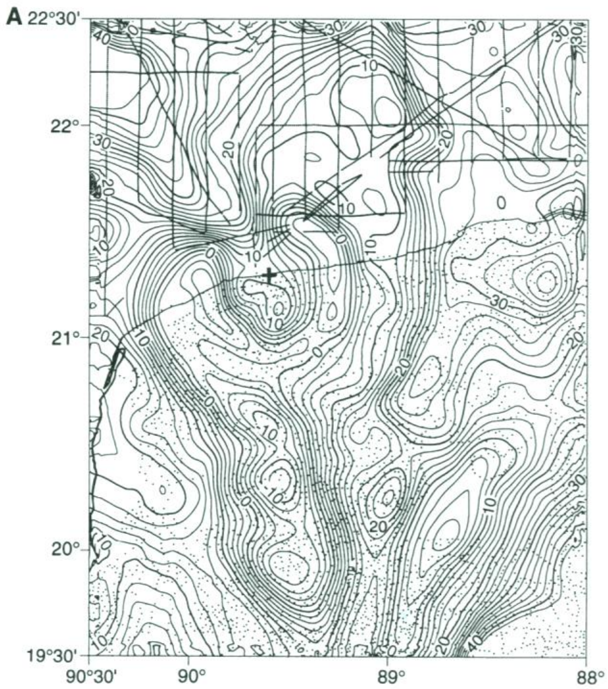

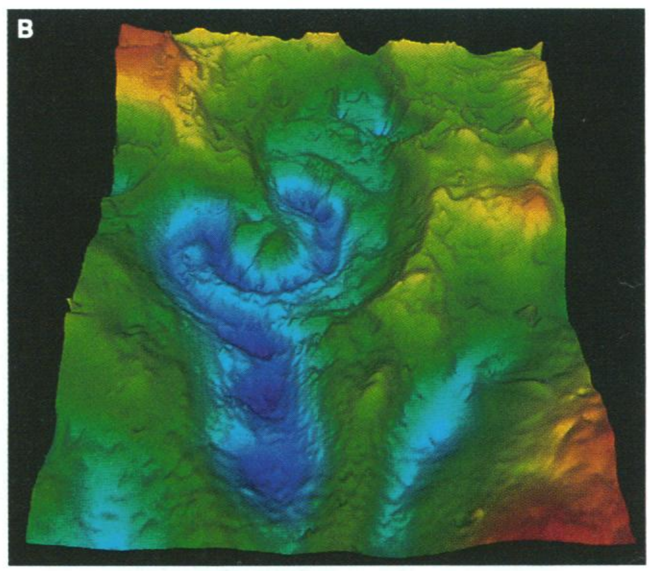

Fig. 2. (**A**) Contoured gravity anomaly data for the region shown in Fig. 1. Center of the Chicxulub impact basin lies at (+). Small dots are gravity stations and offshore measurements (*6*). Before contouring, we smoothed the gridded data by an 11 by 11 (7.2 km by 7.2 km) convolution filter. The contour interval is 2 mgal. (**B**) Relief-shaded gravity anomaly data for the region shown in Fig. 1 viewed obliquely from approximately 60° above the surface looking north. Artificial lighting is from the south.

km in final rim crest diameter (D), indicate that $D_t \simeq 0.5$ to $0.65\ D$ (*11*). For our interpretation of the Chicxulub basin ($D_t \simeq$ 170 km), this relation predicts $D \simeq 260$ to 340 km—in good agreement with the location of the outer ring. This also agrees well with the ~300-km ring diameter predicted by the "square root of 2" analysis summarized in Table 1. Consequently, we believe that ring 4 represents the main basin rim and that the Chicxulub multiring basin is ~300 km in diameter.

A forward model of the average gravity profile (Fig. 4) indicates that the Chicxulub gravity signature is compatible with the interpretation presented above. The ring assignments proposed here place the highly magnetic zone of Penfield and Camargo (*1*) within the central peak ring (ring 1) and the weakly magnetic zone inside the zone of deep deformation (delimited by ring 3), suggesting that the magnetic source is related to deep rocks uplifted, melted, and brecciated in the center of the structure.

The northern part of the basin has not been removed by east-west faulting as was proposed (*2, 4*) on the basis of less comprehensive gravity data. Low amplitude gravity anomalies corresponding to basin rings are evident throughout the northern region (Fig. 3, profile 340). The gravity expression of this part of the basin, however, is partly masked by a strong regional gravity high extending into the crater from the north. This broad feature continues southward past the crater center for over 200 km as a narrow linear gravity low.

During the Jurassic Period, the Yucatán block moved rapidly away from the U.S. Gulf Coast along a counterclockwise, southward path subtending 45° to 65° of arc as the Gulf of Mexico formed (*14*). Because the predrift orientation of the linear gravity feature at Chicxulub is concordant with the Gulf of Mexico rift, we believe that this feature may be related to crustal thinning or incipient rifting associated with the opening Gulf. The broad gravity high in the northern part of the Chicxulub basin could represent mass excesses associated with crustal thinning or volcanic infilling of a rift valley. The linear gravity low (Fig. 3, profile 180) might then reflect thick deposits of relatively low-density volcaniclastic rocks or evaporites located toward the distal and less volcanically active end of the rift zone [for example, figure 2 in (*15*)]. Thick evaporite units have been reported from the Petróleos Mèxicanos drilling sites at the Ticul 1 and the Yucatán 2 wells (*16*) near this feature (Figs. 1 and 2), and similar salt basins are well known to the north of the Gulf of Mexico rift [for example, (*14*)].

At about 300 km in diameter, the Chicxulub multiring basin records one of the largest collisions in the inner solar system since the end of the early period of heavy bombardment almost 4 billion years ago (*17*). The only post–heavy bombardment basin of comparable size identified on the well-studied surfaces of the inner planets and satellites is the 280-km-diameter Mead basin on Venus. Earth probably has not experienced another impact of this magnitude since the development of multicellular life approximately a billion years ago. Such an unusual and energetic event at the K-T boundary (*3*) argues strongly that the effects of this meteorite impact led to the concurrent mass extinction event (*18*). Multiple impact or comet shower models, although not excluded, are not essential. Such impacts would add little to the environmental havoc wreaked by the Chicxulub impact event alone.

Table 1. Radial spacing of rings in the Chicxulub Multiring Impact Basin. Ring assignments are those in Fig. 1. Observed radial distance from crater center is the average ring crest position determined from the number (*N*) of radial profiles that show distinct evidence of the ring. Predicted radial distance applies the "square root of 2" ring spacing rule (*8*) to the central peak ring (Fig. 1, peak 1) to predict positions of the other rings. The disparity between predicted and mean observed distance is given as fraction of predicted value.

Ring	Observed radial distance (km)	*N*	Predicted radial distance (km)	Disparity	Interpretation
1	52.5 ± 5.0	34	52.5		Central peak ring
2	77.1 ± 6.3	28	74.3	0.038	Inner limit to transient crater wall
3	99.6 ± 6.0	33	105.1	0.052	Outer limit to transient crater wall
4	139 ± 11.0	26	148.6	0.063	Basin rim crest

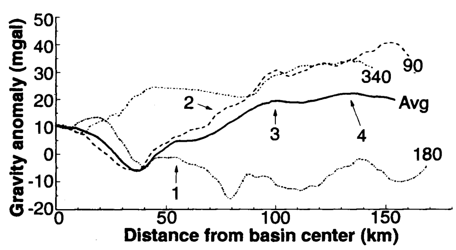

Fig. 3. Gravity profiles through the center of the Chicxulub multiring basin. Avg is the average radial profile constructed from traverses taken at 10° intervals through the center, excluding those affected by the gravity high to the north-northwest (between azimuths 310° and 360°) or the linear gravity depression extending to the south of the structure (between azimuths 170° and 190°). Profile 340 is along azimuth 340° on the crest of the linear gravity high. Profile 180 is along the center of the gravity low extending due south. Profile 90 is a representative profile that shows the change in gradient associated with ring 2. Numbers 1 to 4 indicate basin rings in Fig. 1.

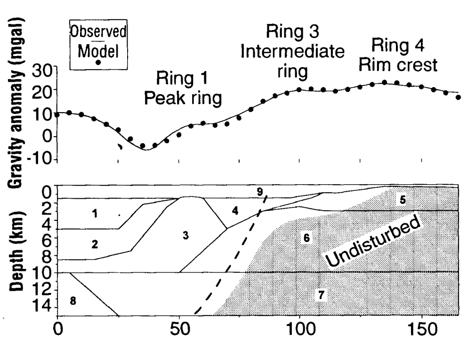

Fig. 4. Forward model of average radial gravity profile (Avg in Fig. 3) of the Chicxulub Impact Basin. The interpretation and density contrasts (g cm^{-3} or 10^{-3} kg m^{-3}) of the modeled rock bodies are as follows: 1, impact melt sheet and melt breccia (0.37); 2, inner allogenic breccia unit (0.25); 3, fractured uplifted crystalline basement (0.31); 4, outer allogenic breccia (0.23); 5, Cretaceous platform sediments (0.18); 6, uppermost crystalline basement (0.40); 7, intermediate basement (0.60); and 8, uplifted deep basement (0.80). All density contrasts are relative to 9, Tertiary carbonate rocks (including ejecta deposits), which have a density of 1.8 to 2.0 g cm^{-3}. Stratigraphy is consistent with drill core data. Unshaded region is the zone of crater disturbance. Bold dashed line shows approximate position of the transient crater boundary in this model.

REFERENCES AND NOTES

1. G. T. Penfield and A. Camargo-Zanaguera, *Soc. Explor. Geophys.* **51**, 37 (1981).
2. A. R. Hildebrand *et al.*, *Geology* **19**, 867 (1991).
3. C. C. Swisher *et al.*, *Science* **257**, 954 (1992); V. L. Sharpton *et al.*, *Nature* **359**, 819 (1992); J. D. Blum *et al.*, *ibid.*, in press.
4. A. R. Hildebrand, M. Pilkington, R. A. F. Grieve, P. B. Robertson, *Lunar Planet. Sci.* **XXIII**, 539 (1992).
5. The digital gridded data set and the gravity image can be obtained from the principal author. A 1:200,000 scale map is being prepared for distribution.
6. Offshore data, from the National Oceanic and Atmospheric Administration, were reduced to free-air anomalies. Onshore data, from the Defense Mapping Agency and 205 stations added from surveys acquired by the Instituto Nacional de Estadistica, Geografica e Informatica from 1990 to 1992, were

reduced to Bouguer anomalies. Ocean depths within the map region do not exceed 100 m and average ~20 m; the distinction between free-air reductions in the offshore data and Bouguer reductions for land stations, therefore, is of little consequence and imparts no meaningful complications to the analysis of the data.
7. H. Akima, *Assoc. Comput. Mach.* **4**, 160 (June 1978); *Rocky Mountain J. Math.* **14**, 41 (winter 1984).
8. This spacing rule can be expressed as $D_N = (\sqrt{2})^{N-1} D_1$ where D_N is the diameter of the Nth ring and D_1 is the diameter of the inner ring. R. J. Pike, *Lunar Planet. Inst. Tech. Rep.* **449**, 46 (1981); ____ and P. D. Spudis, *Earth Moon Planets* **39**, 129 (1987); P. D. Spudis, *Geology of Multiring Basins* (Cambridge Univ. Press, Cambridge, 1993); ____ and V. L. Sharpton, *Lunar Planet. Sci.* **XXIV**, 1339 (1993).
9. R. A. F. Grieve, P. B. Robertson, M. R. Dence, *Geochim. Cosmochim. Acta* **15** (suppl.), 37 (1981); S. K. Croft, *Geochim. Cosmochim. Acta*, *ibid.*, p. 227.
10. The transient crater refers to the deep bowl-shaped cavity produced early in the impact process by excavation plus downward displacement of the target rocks. In large events, more than several kilometers in diameter, this crater form is gravitationally unstable and collapses to form a broader, shallower final crater.
11. H. J. Melosh, *Impact Cratering: A Geologic Process* (Oxford Univ. Press, New York, 1989).
12. P. D. Spudis, B. R. Hawke, P. G. Lucey, *J. Geophys. Res.* **89**, C197 (1984).
13. M. Pilkington and R. A. F. Grieve, *Rev. Geophys.* **30**, 161 (1992).
14. J. L. Pindell, *Tectonics* **4**, 1 (1985); K. Burke, *Annu. Rev. Earth Planet. Sci.* **16**, 201 (1988); S. A. Hall and I. Najmuddin, *GSA Abstr. Programs* **24**, 14 (1992); J. A. Dunbar and D. S. Sawyer, *Tectonics* **6**, 739 (1987).
15. K. Burke and A. J. Whiteman, *Implications of Continental Drift to the Earth Sciences* (Academic Press, London, 1973), vol. 2, p. 735.
16. E. Lopez Ramos, *Geologia de Mexico* (University of Mexico, Mexico City, ed. 2, 1979), vol. 2.
17. W. K. Hartmann, *Icarus* **4**, 157 (1965); *Geochim. Cosmochim. Acta* **12** (suppl.), 155 (1980); G. W. Wetherill, *Science* **228**, 877 (1985).
18. L. W. Alvarez, W. Alvarez, F. Asaro, H. V. Michel, *Science* **208**, 1095 (1980).
19. We thank the Defense Mapping Agency, National Oceanic and Atmospheric Administration, and Instituto Nacional de Estadistica, Geografica e Informatica for providing the gravity data used in this analysis. S. Hokanson drafted Fig. 1. D. Black and B. Schuraytz (Lunar and Planetary Institute) and two anonymous referees provided helpful reviews. This work was conducted through a collaborative research agreement between the Lunar and Planetary Institute and the Instituto de Geofisica, Universidad Nacional Autónoma de México. The Lunar and Planetary Institute is operated by Universities Space Research Association under contract (NASW 4574) with the National Aeronautics and Space Administration. Parts of this work were funded through the National Aeronautics and Space Administration Magellan Guest Investigator and Venus Data Analysis programs (to V.S.) and the Dirección General de Apoyo al Personal Académico, Universidad Nacional Autónoma de México, project number IN106891 (to L.M.). This is Lunar and Planetary Institute contribution number 814.

6 May 1993; accepted 27 July 1993

Chemical Modification of the Photoluminescence Quenching of Porous Silicon

Jeffrey M. Lauerhaas and Michael J. Sailor*

The photoluminescence of porous silicon can be quenched by adsorbates, and the degree of quenching can be tuned by chemical derivatization of the porous silicon surface. Thus, as-prepared porous silicon has a hydrophobic, hydrogen-terminated surface, and the photoluminescence is strongly quenched by ethanol and weakly quenched by water. Mild chemical oxidation (iodine followed by hydrolysis) produces a hydrophilic porous silicon surface. Photoluminescence from this hydrophilic material is quenched to a lesser extent by ethanol and to a greater extent by water, relative to the original surface. This demonstrates that the visible luminescence from porous silicon is highly surface-sensitive, and the surface interactions can be tuned by specific chemical transformations.

The observation of visible photoluminescence (PL) from porous Si has attracted attention for a wide range of applications, including electrooptic (*1*), solar energy conversion (*2*), photodetector (*3*), and chemical sensor devices (*4–7*). Chemical sensors could take advantage of changes in the PL wavelength and intensity that occur in the presence of different chemical adsorbates. For nonreactive molecular adsorbates, the quenching of PL intensity scales roughly with the dipole moment of the chemical species (*5, 6*), so that molecules with large dipole moments like methanol or ethanol quench the PL of porous Si to a large extent (typically >99% loss of PL intensity). The reversible quenching phenomenon has been interpreted as the stabilization of surface traps by alignment of molecular dipoles on the porous Si surface (*5, 6*). An exception to the correlation is water, which does not appreciably quench the PL of porous Si despite its large dipole moment. This observation has been attributed to the hydrophobic nature of the porous Si surface; water does not wet the hydrogen-terminated surface of porous Si, so dipole alignment does not occur.

We tested this postulate by derivatizing the surface of porous Si with hydrophilic O and OH groups. The surface modification reduced the surface hydrophobicity of porous Si, and the PL quenching effect of water was enhanced relative to ethanol. These results clearly show that PL from porous Si is highly dependent on the nature of the interaction of physisorbed molecules with the surface. The chemical "tunability" of this quenching response may be useful in the development of Si-based sensors with a specific adsorbate binding response.

The Fourier-transform infrared (FTIR) spectrum of a freshly etched porous Si wafer (*8*) shows a hydrogen-terminated surface with little to no surface oxide present (Fig. 1A). The proposed reaction (Scheme 1) of I_2 and air

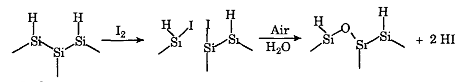

Scheme 1

with porous Si involves an initial attack by I_2 at Si–Si bonds (*9, 10*), which is consistent with the observation that the Si–H and Si–H_2 infrared stretching modes are not reduced significantly on I_2 exposure (Fig. 1B) (*11*). X-ray photoelectron spectroscopy (XPS) of the surface revealed the presence of an iodide species (I $3d_{5/2}$ at 619.9 ± 0.3 eV; Si $2p$ at 102.2 ± 0.3 eV). There was an immediate loss of >99% of the integrated PL intensity on I_2 exposure. Oxidation of the I_2-treated porous Si material in air results in new peaks characteristic of Si–O (at 1100 cm^{-1}), O–Si–H (at 2225 cm^{-1}), and OH (at 3480 cm^{-1}) species (*12*) (Fig. 1C) and recovery of 30% of the original PL intensity (*13*). Initial oxide growth occurs much more rapidly on a porous Si wafer that has been pretreated with I_2 (*10, 14*). Oxide is detectable by FTIR and XPS [O (SiO_2) 1s at 533.0 ± 0.3 eV] on I_2-treated wafers within 5 min of being exposed to air, whereas an untreated porous Si sample requires 122 min in air to grow a comparable oxide thickness. Contact angle measurements on the samples show that the chemically oxidized surface is more hydrophilic than as-formed (H-terminated) porous Si (H_2O drop, advancing contact angles were 112° and 131°, respectively).

The PL intensity of as-formed porous Si was strongly quenched by ethanol vapor (97.4 ± 0.1% drop in integrated intensity, average of nine runs, 95% confidence interval) and weakly quenched by water vapor (11 ± 3%) (Fig. 2A). In contrast, the material that was made more hydrophilic by surface oxidation (Fig. 2B) was

Department of Chemistry, University of California at San Diego, La Jolla, CA 92093.

*To whom correspondence should be addressed.